Supplementary Information for

Deglacial export of pre-aged terrigenous carbon to the Bay of Biscay

Alves et al.

1 Methods

1.1 Sampling and core chronology

Core GeoB23302-2 was recovered from the Celtic Margin, off the English Channel (47°26'N, 8°28'W; 2184 m water depth) (Figure 1 in the main text), with the help of a gravity corer during cruise MSM 79 of the research vessel Maria S. Merian. The core location is in close proximity to the site where core MD95 2002, which has been studied in previous publications (e.g., Ménot et al., 2006; Toucanne et al., 2015), was retrieved (47°27'N, 8°32'W) (see Figure 1 in the main text). The chronology of our 700 cm core was established based on seven radiocarbon accelerator mass spectrometry (^{14}C-AMS) measurements of planktic foraminifera (*G. bulloides* and *N. pachyderma*) picked at specific depths. The preparation and measurement of these samples followed well-established protocols routinely run at the MICADAS ^{14}C laboratory of the Alfred Wegener Institute (AWI) (Mollenhauer et al., 2021). The ^{14}C ages were uploaded to the OxCal software version 4.4.2 (Bronk Ramsey, 1995, 2009a) and, using the P Sequence model, the global marine calibration curve Marine20 (Heaton et al., 2020), and a local marine reservoir correction ΔR of 94 $\pm$ 45 ^{14}C yr (Tisnérat-Laborde et al., 2010), a deposition model was constructed (Bronk Ramsey, 2008; Bronk Ramsey and Lee, 2013). A general outlier analysis was employed to account for possible outliers within the chronological model (Bronk Ramsey, 2009b).

1.2 Elemental analyses

The X-ray fluorescence (XRF) characterization of core GeoB23302-2 was performed using the XRF Core Scanner II (AVAATECH Serial No. 2) at the Center for Marine Environmental Sciences (MARUM), University of Bremen, Germany. Measurements were performed at 1 cm intervals for the upper 3.5 m of the core and at every 2 cm for the remaining section. The scan resolution was set to 1 cm with 2 running rounds, during which the elements were detected with 10 and 30 kV of tube voltage. In order to account for the closed sum effects of water content, grain size and OM amount (e.g., Weltje and Tjallingii, 2008), we report elemental ratios for zirconium (Zr), rubidium (Rb), iron (Fe) and calcium (Ca), i.e., Zr/Rb and Fe/Ca.

1.3 Biomarker analyses and derived indices

Sediment samples taken at 10 cm intervals from core GeoB23302-2 were freeze-dried and homogenized. For each depth, approximately 3 g of sediment were subsampled and underwent ultrasonic extraction with a mixture of dichloromethane:methanol 9:1 (v:v). This step was repeated three times and the total lipid extracts obtained were then saponified with 0.1 M potassium hydroxide (KOH) in methanol:water 9:1 at 80 °C for 2 h. This procedure resulted in the separation of the neutral lipids and *n*-alkanoic acids fractions, which were subsequently extracted using *n*-hexane and dichloromethane (at pH 1), respectively. Next, silica gel chromatography was employed to further split the neutral lipids via elution with *n*-hexane and dichloromethane:methanol 1:1 (v:v), yielding the *n*-alkanes and glycerol dialkyl glycerol tetraether lipids (GDGTs) subfractions, respectively. The *n*-alkane concentrations were measured via gas chromatography (GC) using a 7890A GC (Agilent Technologies) equipped with a flame ionization detector (FID) and DB-5MS fused silica capillary columns (60 m, ID 250 μm, 0.25 μm film coupled to a 5 m, ID 530 μm deactivated fused silica precolumn). Retention times and the comparison with an *n*-alkane standard were used for the identification of different compounds whereas quantifications were achieved through the use of an internal standard (squalane) added to the sample prior to extraction. We calculated *n*-alkane-derived indices, namely the carbon-number preference index ($\mathrm{CPI_{alk}}$) (e.g., Bray and Evans, 1961; Marzi et al., 1993):

$$\mathrm{CPI_{alk}} = \frac{1}{2} \cdot \left(\frac{\mathrm{C_{25}} + \mathrm{C_{27}} + \mathrm{C_{29}} + \mathrm{C_{31}} + \mathrm{C_{33}}}{\mathrm{C_{24}} + \mathrm{C_{26}} + \mathrm{C_{28}} + \mathrm{C_{30}} + \mathrm{C_{32}}} + \frac{\mathrm{C_{25}} + \mathrm{C_{27}} + \mathrm{C_{29}} + \mathrm{C_{31}} + \mathrm{C_{33}}}{\mathrm{C_{26}} + \mathrm{C_{28}} + \mathrm{C_{30}} + \mathrm{C_{32}} + \mathrm{C_{34}}} \right), \quad (1)$$

and the proxy ratio P_{aq} (Ficken et al., 2000):

$$P_{aq} = \frac{C_{23} + C_{25}}{C_{23} + C_{25} + C_{29} + C_{31}}, \quad (2)$$

Hopanes were analyzed via GC coupled with time of flight mass spectrometry (GC-TOF-MS) and such a system consisted of a LECO Pegasus III (LECO Corp., St. Joseph, MI) interfaced to an Agilent 6890 GC which was equipped with a temperature programmable cooled injection system (CIS4, Gerstel). The measurements were performed using the instrumental setup described in Hefter (2008) and identification was achieved through the relative retention times and mass spectra. The sum of m/z 191 and 205 was used for the quantification of homohopane isomers (C_{31}), namely the 17β,21β (H), 22R homohopane, the 17β,21α (H), 22R + 17β,21α (H), 22S homohopanes, the 17α,21β (H), 22R homohopane, and the 17α,21β (H), 22S homohopane. Next, the fractional abundance of hopanes of biological origin, e.g., bacteria-derived hopanes, in relation to their diagenetic isomers was calculated (Meyer et al., 2019):

$$f\beta\beta = \frac{C_{31}\beta\beta R}{C_{31}\beta\beta R + C_{31}\alpha\beta S + C_{31}\alpha\beta R + C_{31}\beta\alpha S + C_{31}\beta\alpha R} \quad (3)$$

The analysis of GDGTs by High Performance Liquid Chromatography (HPLC) was performed on an Agilent 1200 series HPLC system coupled to an Agilent 6120 single quadrupole MS via an atmospheric pressure chemical ionization interface (APCI), broadly following the method described in Hopmans et al. (2016). The chromatographic separation of individual GDGTs was achieved via the use of two UPLC silica columns in series (Waters Acquity BEH HILIC, 2.1 mm x 150 mm, 1.7 μm and a 2.1 mm x 5 mm pre-column of the same material) maintained at 30 °C. Positive-ion APCI-MS and selective ion monitoring (SIM) of (M+H)+ ions (Sinninghe Damsté et al., 2000) or ion-source fragmentation products of OH-GDGTs (Liu et al., 2012) allowed the identification of GDGTs. Quantification was performed with the use of an internal standard (C_{46}-GDGT) added prior to extraction. For this research, we calculated

the branched and isoprenoid tetraether (BIT) index (Hopmans et al., 2004):

$$\mathrm{BIT} = \frac{\mathrm{I} + \mathrm{II} + \mathrm{III}}{\mathrm{I} + \mathrm{II} + \mathrm{III} + \mathrm{cren}} \tag{4}$$

where the roman numerals refer to specific GDGTs characteristic of terrestrial bacteria and cren stands for crenarchaeol, which is derived from marine planktonic Thaumarchaeota.

1.4 Bulk radiocarbon analyses

The total OM in the sediment was ^{14}C dated following the protocol described in Mollenhauer et al. (2021). Sediment samples were weighed into silver boats to yield 1 mg OC (ELEMENTAR) and three drops of 6 M distilled hydrochloric acid (HCl) were added for the removal of carbonates. The reaction happened at 60 °C, until the acid evaporated, and was repeated three times. Next, the silver boats containing the samples were folded into a tin boat (ELEMENTAR). Samples were then combusted at 950 °C in an elemental analyzer (Elementar vario Isotope) and graphitized in an automated graphitization system (AGE-3; Ionplus AG; Wacker et al., 2010). Results were normalized to modern oxalic acid II standard (NIST 4990C).

1.5 Compound-specific radiocarbon analyses (CSRA)

Soxhlet extraction was employed for the compound-specific ^{14}C dating of high molecular weight *n*-alkanoic acids. For that purpose, approximately 100 g of freeze-dried and homogenized sediment taken from selected depths in core GeoB23302-2 were extracted for 48 h using a mixture of dichloromethane:methanol 9:1 (v:v). Total lipid extracts were saponified with 0.1 M KOH in methanol:water 9:1 at 80 °C for 2 h and the *n*-alkanoic acids were recovered from the saponified solution using *n*-hexane at pH 1. Next, *n*-alkanoic acids were methylated at 80 °C overnight in a nitrogen atmosphere with HCl and methanol of known ^{14}C signature to yield the fatty acid methyl esters (FAMEs) that were later extracted with *n*-hexane. Silica gel chromatography was employed to separate FAMEs from polar compounds. The *n*-$C_{26:0}$, *n*-$C_{28:0}$ and *n*-$C_{30:0}$ alkanoic acids underwent purification via preparative capillary GC (PC-GC; Eglinton et al., 1996) on an Agilent HP6890N GC with a Gerstel Cooled Injection System (CIS) con-

nected to a Gerstel preparative fraction collector (Kusch et al., 2010). A Restek Rxi-1ms fused silica capillary column (30 m, 0.53 mm diameter, 1.5 μm film thickness) equipped the GC. Injection was performed stepwise with 5 μL per injection and, at the end of the process, the purity of the FAMEs was checked by analyzing aliquots of the samples via GC-FID. The purified FAMEs were transferred to tin capsules (25 μL volume; ELEMENTAR) using dichloromethane, dried on a hot plate at 40 °C and packed. An Elementar vario ISOTOPE EA (Elemental Analyzer) was used for the combustion of the samples, generating CO_2 with carbon isotopic ratios directly determined by the connected MICADAS system. Reference standards (oxalic acid II; NIST 4990C) and blanks (phthalic anhydride; Sigma-Aldrich 320064) had their ^{14}C content measured together with the samples. The BATS software (Wacker et al., 2010) was used for blank corrections and standard normalization and the final results are reported as fraction modern carbon (F_m).

1.6 Assessment and correction of CSRA procedure blank

The preparation procedures for CSRA introduce exogenous C, i.e., contaminants, to samples. The degree of contamination varies according to the methods employed and, in our case, processes such as column bleed and carry-over may contribute to this. For this reason, assessing the F_m and the size of the blank (F_{mblank} and m_{blank}, respectively) is essential for accurate results. Here, in-house reference samples of ^{14}C-free Messel Shale ($F_m = 0$) and modern apple peel ($F_m = 1.029 \pm 0.001$) underwent the same pre-treatment as samples of unknown age and their results were used for blank correction following the method outlined in Sun et al. (2020). Isotopic mass balance was employed in order to make a correction for the methyl group added during the derivatization of the samples. Uncertainties were fully propagated.

1.7 Pre-depositional ^{14}C ages of terrigenous compounds

The $\Delta^{14}C$ values of the *n*-alkanoic acids analysed here were corrected for radioactive decay between 1950 and 2021, which is the year of measurement. These values were then used to calculate the $\Delta^{14}C$ values at the time of deposition:

$$\Delta^{14}C_{initial} = \left[\left(\frac{\Delta^{14}C}{1000} + 1\right) \cdot e^{\lambda t} - 1\right] \cdot 1,000 \quad (5)$$

where λ is a decay constant (1/8,267 yr^{-1}) and t is the time of deposition. The $\Delta^{14}C$ values of the

atmosphere contemporaneous with the compounds ($\Delta^{14}C_{atm}$) were obtained from comparison with the IntCal20 dataset (Reimer et al., 2020) using the age ranges given by the deposition model for the respective sediment layers. Finally, pre-depositional ^{14}C ages for the *n*-alkanoic acids were given by:

$$A = -8,033 \cdot \ln\left(\frac{1+\Delta^{14}C_{initial}/1,000}{1+\Delta^{14}C_{atm}/1,000}\right) \quad (6)$$

These calculations follow the method outlined in Schefuß et al. (2016) and later in Winterfeld et al. (2018), where more details can be found.

1.8 Stable isotope analyses

Carbon stable isotope ($\delta^{13}C$) analyses were carried out on acidified samples (Ag capsules, HCl, 1.5 M) in order to remove the inorganic C (Nieuwenhuize et al., 1994). Analyses were performed using a Thermo Scientific DELTA Q Isotope Ratio Mass Spectrometer coupled to a Thermo Scientific FLASH 2000 CHNS/O Analyzer via Conflo III at the Stable Isotope Laboratory of ISP-CNR. $\delta^{13}C$ data are expressed in the conventional delta notation (‰). Isotopic data were calibrated using the IAEA reference material IAEA-CH7 polyethylene, -32.15‰vs VPDB). Throughout the runs, we used other standards with a sediment matrix routinely used in the laboratory to check the reproducibility of measurements. The standard deviation for $\delta^{13}C$ measurements was lower than $\pm$0.1‰based on replicates of sediment standards.

1.9 Mixing models

Petrogenic OC (OC_{petro}) as well as terrestrial ($OC_{ter-bio}$) and marine ($OC_{mar-bio}$) biospheric OC were used as end-members. While OC_{petro} means ^{14}C-free OC, $OC_{ter-bio}$ and $OC_{mar-bio}$ typically comprise terrestrial and marine OM, respectively, with a ^{14}C content higher than that of OC_{petro}. The $\Delta^{14}C$ values of the bulk samples were corrected for radioactive decay between 1950 and 2021 and $\Delta^{14}C_{initial}$ values were calculated using Equation 5. The $\Delta^{14}C$ value of OC_{petro} was defined as -1000‰, but for $OC_{ter-bio}$ and $OC_{mar-bio}$ $\Delta^{14}C$ temporal variations were taken into account. The $\Delta^{14}C$ values measured for the *n*-alkanoic acids were used to calculate the initial $\Delta^{14}C$ values of $OC_{ter-bio}$ using Equation 5, with the standard deviations of the averaged values being taken as the uncertainties. Simulations of the ^{14}C marine reservoir age (R) at the times of deposition in our study region (Butzin et al., 2017) were added to the IntCal20 atmospheric record to derive ^{14}C ages for the Bay of Biscay. These were

subsequently converted to the $\Delta^{14}C$ values of $OC_{mar-bio}$ and the uncertainties in Marine20 were used as a first approximation. Measurements of $\delta^{13}C$ in peat samples from Northeast Germany (Jahns, 2007) were used as the $\delta^{13}C$ value of $OC_{ter-bio}$ (-27.4 $\pm$ 1.7 ‰) and a $\delta^{13}C$ value previously reported for the Biscay Shelf (Fontugne and Jouanneau, 1987) was assigned to $OC_{mar-bio}$ (-20.5 $\pm$ 0.2 ‰). Finally, for OC_{petro}, brown coal $\delta^{13}C$ values from the German Lower Rhine Embayment were used in our model (-25.8 $\pm$ 0.3 ‰; Lücke et al., 1999). This is because the CPI_{alk} and the $f\beta\beta$ records do not point to a fully petrogenic source.

Considering the end-members discussed above, we used the MixSIAR package version 3.1.12 (Stock et al., 2018) within the R programming environment to run a Bayesian mixing model to determine the contributions of each source to our bulk samples.

2 Supplementary Figures

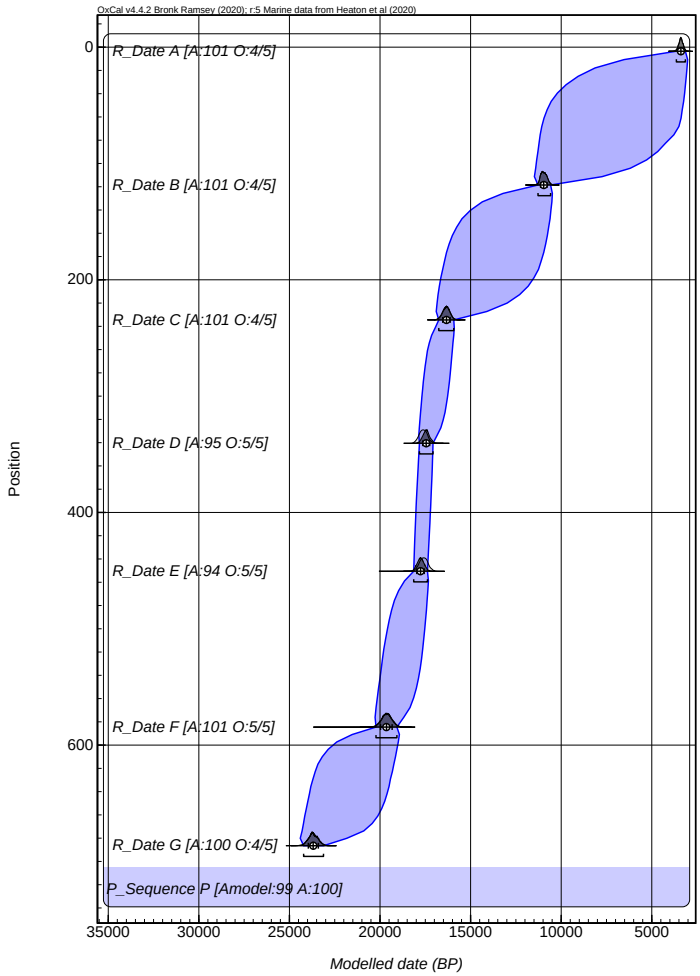

Figure S 1. Age-depth model for core GeoB23302-2. Sample depth (position) is given in cm.

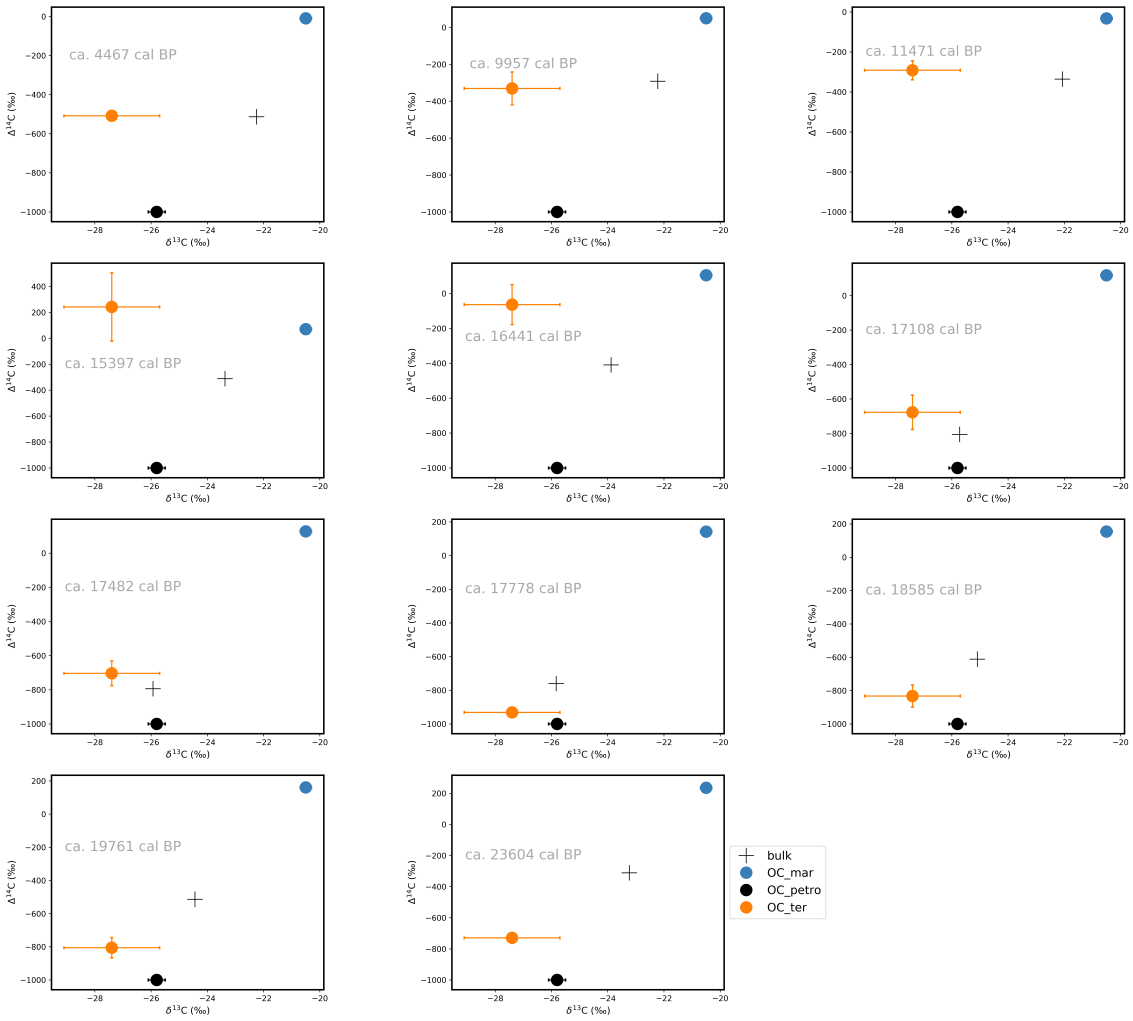

Figure S 2. Dual-isotope mixing model to disentangle the contributions of biospheric terrestrial C, petrogenic C and biospheric marine C to bulk OM samples.

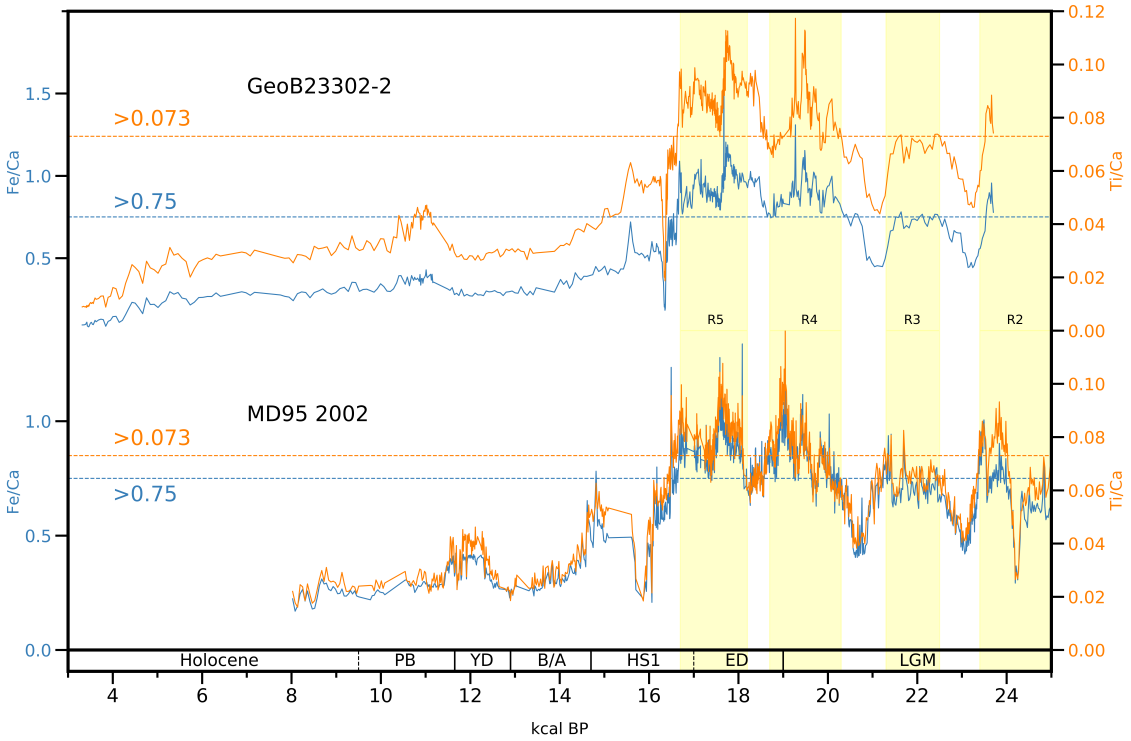

Figure S 3. XRF-Fe/Ca and Ti/Ca data for cores GeoB23302-2 and MD95 2002 (Toucanne et al., 2015) allow for the identification of runoff events (R2-R5) that may have enhanced erosive processes and contributed ^{14}C-depleted OM to the continental shelf.

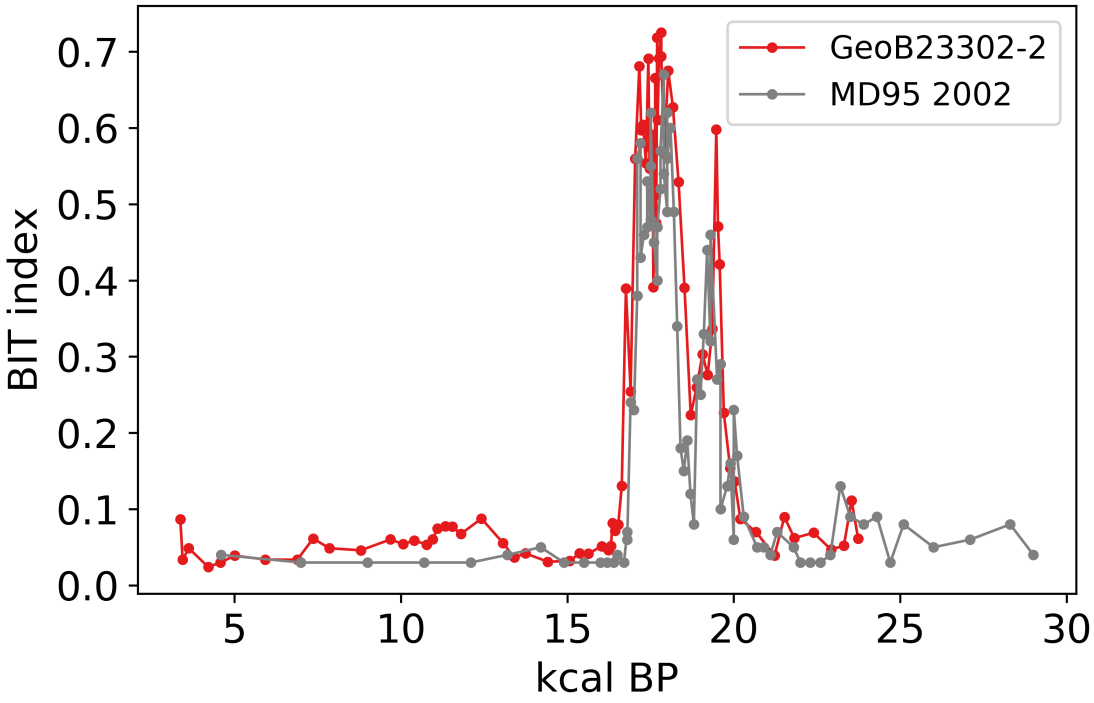

Figure S 4. BIT index data for cores GeoB23302-2 and MD95 2002 (Ménot et al., 2006).

3 Considerations on the fββ proxy

In this study we have followed Meyer et al. (2019) and Wu et al. (2022) and applied the fββ indicator to track possible petrogenic contributions to the OM in core GeoB23302-2 (see Equation 4 in the manuscript). The index is based on the relative abundance of the so-called biologic (i.e., 17β,21β(H) and 22R) and geologic isomers (i.e., 17β,21αS, 17β,21αR, 17α,21βS and 17α,21βR) (e.g., Einsminger et al., 1972; Rohmer et al., 1992). The latter are usually the result of diagenetic and temperature-induced processes affecting the former and leading to a more thermally stable configuration (e.g., Seifert and Moldowan, 1980; Mackenzie and Mackenzie, 1983; Rohmer et al., 1992; Sinninghe Damsté et al., 1995; Van Duin et al., 1997; Kolaczkowska et al., 1990; Peters and Moldowan, 1993; Lockhart et al., 2008). The hopane abundance in core GeoB23302-2 shows that the concentration of the biosynthesized 31ββ isomer, typically present in immature fresh OM, is positively correlated with that of 31αβR, which is commonly found in petrogenic sources (e.g., Peters and Moldowan, 1993; Sinninghe Damsté et al., 1995; Lockhart et al., 2008). This means that increases in the input of the 31αβR compound rather than transformations from ββ to αβ and βα isomers are responsible for decreases in the fββ record. The geochemical signature of peat shows a high abundance of the 31αβR compound but comparatively low values for the 31αβS epimer (Inglis et al., 2018), which is reflected in our data. Contrary to what has been observed in Meyer et al. (2019), where low fββ and relatively high S/(S+R) values indicate petrogenic input, we see low fββ and low S/(S+R) values (Figure 5). Therefore, in this study, the fββ proxy does not reflect petrogenic input but rather the influx of peat/lignite material.

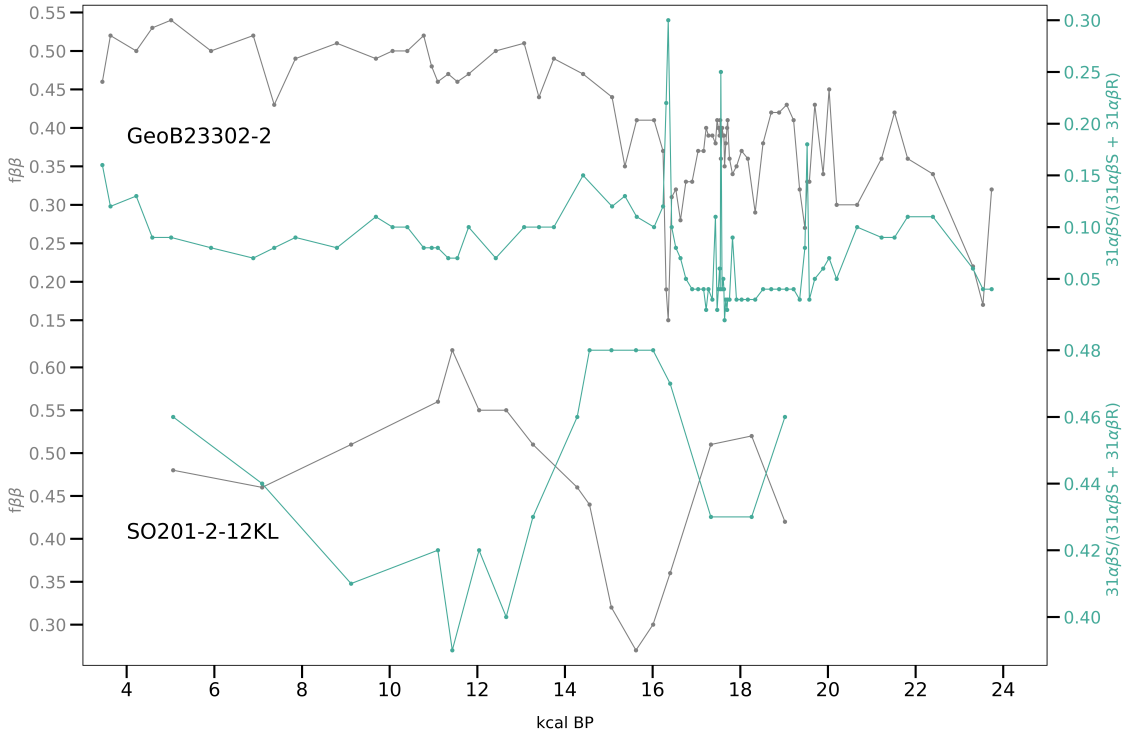

Figure S 5. Records of the fββ indicator and the relative abundance of the 31αβS and R compounds of cores GeoB23302-2 and SO201-2-12KL (Meyer et al., 2019) for comparison.

References

Bray, E. E. and Evans, E. D. (1961). Distribution of n-paraffins as a clue to recognition of source beds. *Geochimica et Cosmochimica Acta*, 22(1):2–15.

Bronk Ramsey, C. (1995). Radiocarbon calibration and analysis of stratigraphy: the OxCal program. *Radiocarbon*, 37(2):425–430.

Bronk Ramsey, C. (2008). Deposition models for chronological records. *Quaternary Science Reviews*, 27(September 2006):42–60.

Bronk Ramsey, C. (2009a). Bayesian analysis of radiocarbon dates. *Radiocarbon*, 51(1):337–360.

Bronk Ramsey, C. (2009b). Dealing with outliers and offsets in radiocarbon dating. *Radiocarbon*, 51(3):1023–1045.

Bronk Ramsey, C. and Lee, S. (2013). Recent and Planned Developments of the Program OxCal. *Radiocarbon*, 55(3–4):720–730.

193 Butzin, M., Köhler, P., and Lohmann, G. (2017). Marine radiocarbon reservoir age simulations for the past 50,000 years.
194 *Geophysical Research Letters*, 44(16):8473–8480.

195 Eglinton, T. I., Aluwihare, L. I., Bauer, J. E., Druffel, E. R., and McNichol, A. P. (1996). Gas chromatographic isolation
196 of individual compounds from complex matrices for radiocarbon dating. *Analytical Chemistry*, 68(5):904–912.

197 Einsminger, A., Albrecht, P., and Ourisson, G. (1972). Homohopane in Messel Oil Shale: First Identification of a C31
198 Pentacyclic Triterpane in Nature. *Tetrahedron Letters*, (36):3861–3864.

199 Ficken, K. J., Li, B., Swain, D. L., and Eglinton, G. (2000). An n-alkane proxy for the sedimentary input of sub-
200 merged/floating freshwater aquatic macrophytes. *Organic Geochemistry*, 31(7-8):745–749.

201 Fontugne, M. R. and Jouanneau, J. M. (1987). Modulation of the particulate organic carbon flux to the ocean by
202 a macrotidal estuary: Evidence from measurements of carbon isotopes in organic matter from the Gironde system.
203 *Estuarine, Coastal and Shelf Science*, 24(3):377–387.

204 Heaton, T. J., Köhler, P., Butzin, M., Bard, E., Reimer, R. W., Austin, W. E., Bronk Ramsey, C., Grootes, P. M., Hughen,
205 K. A., Kromer, B., Reimer, P. J., Adkins, J., Burke, A., Cook, M. S., Olsen, J., and Skinner, L. C. (2020). Marine20 -
206 The Marine Radiocarbon Age Calibration Curve (0-55,000 cal BP). *Radiocarbon*, 62(4):779–820.

207 Hefter, J. (2008). Analysis of Alkenone Unsaturation Indices with Fast Gas Chromatography/Time-of-Flight Mass Spec-
208 trometry. *Analytical Chemistry*, 80:2161–2170.

209 Hopmans, E. C., Schouten, S., and Sinninghe Damsté, J. S. (2016). The effect of improved chromatography on GDGT-
210 based palaeoproxies. *Organic Geochemistry*, 93:1–6.

211 Hopmans, E. C., Weijers, J. W., Schefuß, E., Herfort, L., Sinninghe Damsté, J. S., and Schouten, S. (2004). A novel
212 proxy for terrestrial organic matter in sediments based on branched and isoprenoid tetraether lipids. *Earth and Planetary*
213 *Science Letters*, 224(1-2):107–116.

214 Inglis, G. N., Naafs, B. D. A., Zheng, Y., McClymont, E. L., Evershed, R. P., and Pancost, R. D. (2018). Distribu-
215 tions of geohopanoids in peat: Implications for the use of hopanoid-based proxies in natural archives. *Geochimica et*
216 *Cosmochimica Acta*, 224:249–261.

217 Jahns, S. (2007). Palynological investigations into the Late Pleistocene and Holocene history of vegetation and settlement
218 at the Löddigsee, Mecklenburg, Germany. *Vegetation History and Archaeobotany*, 16(2-3):157–169.

219 Kolaczkowska, E., Slougui, N. E., Watt, D. S., Maruca, R. E., and Michael Moldowan, J. (1990). Thermodynamic stability
220 of various alkylated, dealkylated and rearranged 17α- and 17β-hopane isomers using molecular mechanics calculations.
221 *Organic Geochemistry*, 16(4-6):1033–1038.

222 Kusch, S., Rethemeyer, J., Schefuß, E., and Mollenhauer, G. (2010). Controls on the age of vascular plant biomarkers in
223 Black Sea sediments. *Geochimica et Cosmochimica Acta*, 74(24):7031–7047.

Liu, X.-l., Lipp, J. S., Simpson, J. H., Lin, Y.-s., Summons, R. E., and Hinrichs, K.-u. (2012). Mono- and dihydroxyl glycerol dibiphytanyl glycerol tetraethers in marine sediments : Identification of both core and intact polar lipid forms. *Geochimica et Cosmochimica Acta*, 89:102–115.

Lockhart, R. S., Meredith, W., Love, G. D., and Snape, C. E. (2008). Release of bound aliphatic biomarkers via hydropyrolysis from Type II kerogen at high maturity. *Organic Geochemistry*, 39(8):1119–1124.

Lücke, A., Helle, G., Schleser, G. H., Figueiral, I., Mosbrugger, V., Jones, T. P., and Rowe, N. P. (1999). Environmental history of the German Lower Rhine Embayment during the Middle Miocene as reflected by carbon isotopes in brown coal. *Palaeogeography, Palaeoclimatology, Palaeoecology*, 154(4):339–352.

Mackenzie, A. and Mackenzie, D. (1983). Isomerization and aromatization of hydrocarbons in sedimentary basins formed by extension. *Geological Magazine*, 120(5):417–470.

Marzi, R., Torkelson, B. E., and Olson, R. K. (1993). A revised carbon preference index. *Organic Geochemistry*, 20(8):1303–1306.

Ménot, G., Bard, E., Rostek, F., Weijers, J. W. H., Hopmans, E. C., Schouten, S., and Damste, J. S. S. (2006). Early Reactivation of European Rivers During the Last Deglaciation. *Science*, 313(September):1623–1625.

Meyer, V. D., Hefter, J., Köhler, P., Tiedemann, R., Gersonde, R., Wacker, L., and Mollenhauer, G. (2019). Permafrost-carbon mobilization in Beringia caused by deglacial meltwater runoff, sea-level rise and warming. *Environmental Research Letters*, 14(8).

Mollenhauer, G., Grotheer, H., Gentz, T., Bonk, E., and Hefter, J. (2021). Standard operation procedures and performance of the MICADAS radiocarbon laboratory at Alfred Wegener Institute (AWI), Germany. *Nuclear Instruments and Methods in Physics Research, Section B: Beam Interactions with Materials and Atoms*, 496(April):45–51.

Nieuwenhuize, J., Maas, Y., and Middelburg, J. (1994). Rapid Analysis of Organic Carbon.Pdf. *Marine Chemistry*, 45:217–224.

Peters, K. and Moldowan, J. (1993). *The Biomarker Guide*. Prentice Hall, Englewood cliffs, NJ.

Reimer, P. J., Austin, W. E., Bard, E., Bayliss, A., Blackwell, P. G., Bronk Ramsey, C., Butzin, M., Cheng, H., Edwards, R. L., Friedrich, M., Grootes, P. M., Guilderson, T. P., Hajdas, I., Heaton, T. J., Hogg, A. G., Hughen, K. A., Kromer, B., Manning, S. W., Muscheler, R., Palmer, J. G., Pearson, C., Van Der Plicht, J., Reimer, R. W., Richards, D. A., Scott, E. M., Southon, J. R., Turney, C. S., Wacker, L., Adolphi, F., Büntgen, U., Capano, M., Fahrni, S. M., Fogtmann-Schulz, A., Friedrich, R., Köhler, P., Kudsk, S., Miyake, F., Olsen, J., Reinig, F., Sakamoto, M., Sookdeo, A., and Talamo, S. (2020). The IntCal20 Northern Hemisphere Radiocarbon Age Calibration Curve (0-55 cal kBP). *Radiocarbon*, 62(4):725–757.

Rohmer, M., Bisseret, P., and Neunlist, S. (1992). The hopanoids, prokaryotic triterpenoids and precursors of ubiquitous molecular fossils. In *Biological Markers in Sediments and Petroleum*, pages 1–17. Prentice Hall, Englewood cliffs, NJ.

256 Schefuß, E., Eglinton, T. I., Spencer-Jones, C. L., Rullkötter, J., De Pol-Holz, R., Talbot, H. M., Grootes, P. M., and
257 Schneider, R. R. (2016). Hydrologic control of carbon cycling and aged carbon discharge in the Congo River basin.
258 *Nature Geoscience*, 9(9):687–690.

259 Seifert, W. K. and Moldowan, J. M. (1980). The effect of thermal stress on source-rock quality as measured by hopane
260 stereochemistry. *Physics and Chemistry of the Earth*, 12(C):229–237.

261 Sinninghe Damsté, J. S., Hopmans, E. C., Pancost, R. D., Schouten, S., and Geenevasen, J. A. (2000). Newly discovered
262 non-isoprenoid glycerol dialkyl glycerol tetraether lipids in sediments. *Chemical Communications*, 17:1683–1684.

263 Sinninghe Damsté, J. S., Van Duin, A. C., Hollander, D., Kohnen, M. E., and De Leeuw, J. W. (1995). Early diagenesis of
264 bacteriohopanepolyol derivatives: Formation of fossil homohopanoids. *Geochimica et Cosmochimica Acta*, 59(24):5141–
265 5157.

266 Stock, B. C., Jackson, A. L., Ward, E. J., Parnell, A. C., Phillips, D. L., and Semmens, B. X. (2018). Analyzing mixing
267 systems using a new generation of Bayesian tracer mixing models. *PeerJ*, 2018(6):1–27.

268 Sun, S., Meyer, V. D., Dolman, A. M., Winterfeld, M., Hefter, J., Dummann, W., McIntyre, C., Montluçon, D. B.,
269 Haghipour, N., Wacker, L., Gentz, T., Van Der Voort, T. S., Eglinton, T. I., and Mollenhauer, G. (2020). 14C
270 Blank Assessment in Small-Scale Compound-Specific Radiocarbon Analysis of Lipid Biomarkers and Lignin Phenols.
271 *Radiocarbon*, 62(1):207–218.

272 Tisnérat-Laborde, N., Paterne, M., Métivier, B., Arnold, M., Yiou, P., Blamart, D., and Raynaud, S. (2010). Variability of
273 the northeast Atlantic sea surface Δ14C and marine reservoir age and the North Atlantic Oscillation (NAO). *Quaternary*
274 *Science Reviews*, 29(19-20):2633–2646.

275 Toucanne, S., Soulet, G., Freslon, N., Silva Jacinto, R., Dennielou, B., Zaragosi, S., Eynaud, F., Bourillet, J. F., and
276 Bayon, G. (2015). Millennial-scale fluctuations of the European Ice Sheet at the end of the last glacial, and their
277 potential impact on global climate. *Quaternary Science Reviews*, 123:113–133.

278 Van Duin, A. C., Sinninghe Damsté, J. S., Koopmans, M. P., Van De Graaf, B., and De Leeuw, J. W. (1997). A kinetic
279 calculation method of homohopanoid maturation: Applications in the reconstruction of burial histories of sedimentary
280 basins. *Geochimica et Cosmochimica Acta*, 61(12):2409–2429.

281 Wacker, L., Christl, M., and Synal, H. A. (2010). Bats: A new tool for AMS data reduction. *Nuclear Instruments and*
282 *Methods in Physics Research Section B: Beam Interactions with Materials and Atoms*, 268(7-8):976–979.

283 Weltje, G. J. and Tjallingii, R. (2008). Calibration of XRF core scanners for quantitative geochemical logging of sediment
284 cores: Theory and application. *Earth and Planetary Science Letters*, 274(3-4):423–438.

285 Winterfeld, M., Mollenhauer, G., Dummann, W., Köhler, P., Lembke-Jene, L., Meyer, V. D., Hefter, J., McIntyre, C.,
286 Wacker, L., Kokfelt, U., and Tiedemann, R. (2018). Deglacial mobilization of pre-aged terrestrial carbon from degrading
287 permafrost. *Nature Communications*, 9(1).

Wu, J., Mollenhauer, G., Stein, R., Köhler, P., Hefter, J., Fahl, K., Grotheer, H., Wei, B., and Nam, S.-i. (2022). Deglacial release of petrogenic and perma- frost carbon from the Canadian Arctic impacting the carbon cycle. *Nature Communications*, 13:1–11.